Journal of the Serbian Chemical Society
JSCS-info@shd.org.rs • www.shd.org.rs/JSCS
J. Serb. Chem. Soc. 91 (0) 1–15 (2026)
JSCS–13441
Original scientific paper
Published 5 Feb 2026

Bimetallic polyaniline/silver–palladium nanocomposite for rapid and sustainable degradation of eosin yellow dye from wastewater

NOOR ZAMAN[1], FARAH NAZ TALPUR[1], ABDUL QADEER LAGHARI[2]*, JAMEEL BAIG[1], ARSHAD IQBAL[3], SHOUKAT ALI NOONARI[4], ZULFIQAR ALI BHATTI[2], AMANA BALOCH[1], IMRAN HASSAN AFARIDI[1] and MASROOR ABRO[2]

[1]National center of Excellence in Analytical chemistry, University of Sindh, Jamshoro, Sindh, Pakistan, [2]Process Simulation and Modeling Research Group, Chemical Engineering Department, Mehran University of Engineering and Technology Jamshoro, Sindh, Pakistan, [3]Chemical Engineering Department, Dawood University of Engineering and Technology, Karachi, Pakistan and [4]Department of Mechanical Engineering, Isra University, Hyderabad, Sindh, Pakistan

(Received 2 July, revised 14 August, accepted 1 October 2025)

Abstract: Eosin yellow (EY), a synthetic xanthene dye, is recognized for its high toxicity, posing serious threats to human health and aquatic environments. Chronic exposure to EY can result in skin irritation, respiratory disorders, and potential long-term organ damage due to its persistent and bioaccumulative nature. In this study, a polyaniline-based silver–palladium nanocomposite (PANI/Ag–Pd) was synthesized *via* the co-precipitation method and employed as an efficient nanocatalyst for the degradation of EY dye. The structural, morphological and elemental properties of the synthesized nanocomposite were characterized using UV–Vis spectroscopy, Fourier-transform infrared spectroscopy (FTIR), scanning electron microscopy (SEM) and energy-dispersive X-ray spectroscopy (EDX). The UV–Vis and FTIR analyses confirmed the formation of the PANI/Ag–Pd nanocomposite with a notable red shift, indicating electronic interaction among the constituents. SEM images demonstrated the successful incorporation of Ag and Pd nanoparticles into the PANI matrix, while EDX confirmed the elemental composition. The nanocomposite exhibited remarkable photocatalytic performance under microwave irradiation, achieving up to 96.63 % degradation of EY dye. This study highlights the potential of PANI/Ag–Pd nanocomposites as a promising nanocatalyst for water purification. These findings contribute to the development of polymer-stabilized nanomaterials as effective candidates for the remediation of dye-contaminated wastewater.

Keywords: wastewater treatment; nanocomposite; degradation; EY dye.

* Corresponding author. E-mail: abdul.qadeer@admin.muet.edu.pk
https://doi.org/10.2298/JSC250702073Z

INTRODUCTION

In recent decades, advanced materials such as nanomaterials, polymer-based systems and hybrids have attracted increasing scientific interest due to their exceptional chemical and physical properties.[1–4] Dyes are classified into azoic, reactive, vat, sulphur, acidic, basic, disperse and direct.[5] Over 10,000 commercially existing dyes and 1 Mt dyes are prepared annually, containing 50 % as a textile dye.[6] About 10 % of dyestuff is discarded after drying and processing.[7] 2 % of the dye component entered the aqueous matter and caused pollution.[8] Many are toxic and discharged into wastewater untreated, often in high concentrations.[9] Long-term usage of water-containing dyes causes severe health issues. Dyes are carcinogenic and mutagenic. These dyes have been associated with carcinogenic effects in the kidney, bladder and liver, and may also contribute to skin irritation and respiratory complications.[10,11] The cationic/anionic nature dyes leads to reduced amount of oxygen in the water, which is fatal for humans and aquatic life.[12] Several methods are being investigated for dyes removal from wastewater, like microbial-electro-fenton (MEF) technology,[13] catalytic degradation,[14] adsorption,[15] coagulation–flocculation,[16] electrochemical treatment,[17] reverse osmosis[18] and ion exchange.[19]

Among various treatment methods, advanced oxidation processes (AOPs) have shown promise.[20] Photocatalytic degradation using metals and metal oxides like Ag, Pd, TiO_2, ZnO and WO_3 has been explored,[21] often enhanced with additives like $NaBH_4$ to boost dye decolonization efficiency under sunlight.[22]

Polymers have recently emerged as promising alternatives to conventional nanomaterials due to their adjustable surface functionalities, superior mechanical strength, high surface area, uniform pore distribution and easy regeneration properties. Polymers such as polyaniline **(**PANI), polythiophene (PTh)**,** polyethyleneimine (PEI) and polypyrrole (PPy) have gained significant research interest for developing metal–polymer nanocomposites. These hybrid materials have broad applications in photocatalysis, sensing, adsorption, thermoelectric, electromagnetics and batteries, as well as electroluminescent and electromechanical systems. Among these, PANI is one of the most widely explored conductive polymers, owing to its electron-rich structure, environmental stability, low cost and ease of synthesis and processing.[23,24] Its multifunctionality has enabled its use in a broad range of technologies such as lithium-ion batteries,[25] flexible electronics,[26] anti-corrosion coatings,[27] wastewater treatment, dye removal[28] and printed electronics.[29] The PANI/Ag–Pd system offers several advantages over traditional catalysts. The conductive PANI matrix enhances electron transfer and provides high surface area for dye adsorption, while Ag and Pd nanoparticles create abundant active sites and exhibit strong catalytic synergy. This combination enables faster degradation rates, lower energy input and higher stability compared to single-metal or conventional catalysts. Additionally, the nanocom-

posite is reusable, environmentally benign, and effective under mild conditions, making it a sustainable alternative for wastewater treatment applications.

It is often used as a π-conjugated polymer base for integrating wide-bandgap semiconductors such as metal oxides and sulfides. These composites demonstrate enhanced photocatalytic, optical and photoelectric characteristic.[30] Additionally, PANI acts as a proficient electron donor and hole transporter under UV–Vis light exposure. When combined with high-bandgap metals like Ag, Fe, TiO_2 or ZnO, PANI facilitates electron excitation under photon irradiation. These photoexcited electrons transferred to the conduction band of the metal components, promoting the generation of reactive species such as superoxide ($O_2^{-\bullet}$) and hydroxyl radical ($^{\bullet}OH$) through reactions with water and oxygen, which then drive the degradation of eosin yellow (EY) dye. In addition to experimental strategies, theoretical modeling and statistical optimization are essential for developing sustainable treatment processes. Statistical and predictive modeling approaches, such as response surface methodology (RSM), enable systematic evaluation of multiple operating variables, reduce experimental effort and predict interactions that are often overlooked in conventional one-variable-at-a-time studies. By optimizing key parameters, RSM ensures maximum degradation efficiency under practical conditions, strengthening the reliability and scalability of nanocomposite-based wastewater remediation.

In this work, *in-situ* synthesis of a PANI/Ag–Pd nanocomposite demonstrating excellent catalytic behavior, was performed. EY degradation performance of PANI/Ag–Pd nanocomposite was investigated under different composite dose, dye dose, pH and reaction time. Subsequently, RSM was performed with the purpose of process optimization. PANI/Ag–Pd nanocomposite could be a potential candidate in dye removal process owing to its easy synthesis, low production cost and high degradation efficiency.

EXPERIMENTAL

Chemicals and reagents

All the laboratory grade chemicals, glassware and other items were bought from Sigma Aldrich. Aniline (99.95 %) was used as precursor to synthesize for polyaniline polymer. Hydrazine (98 %) was used as strong reducing agent as facilitator for synthesis of silver–palladium nanoparticles. Silver nitrate (99.8 %) and palladium(II) chloride, (99.999 %) were used for synthesis for silver–palladium nanoparticles. Ammonium persulfate (98 %) was used as strong oxidizing agent as facilitator for synthesis of PANI/Ag–Pd nanocomposite. Sulfuric acid (98 %) was added as a proton source to form the conductive emeraldine salt of polyaniline, while protonated aniline exhibits a higher oxidation potential than neutral aniline, thus delaying the onset of polymerization**.** Eosin yellow (EY) dye (99 %) was used as degradation agent. Sodium borohydride (98 %) was used to donate hydrogen atoms (or electrons), breaking down the dye molecules into less harmful by products.

Synthesis of PANI/Ag–Pd

PANI was synthesized by dissolving 1.86 mL of aniline in 200 mL of 0.1 M H_2SO_4, followed by the dropwise addition of 10 mL of 5 M APS and stirring for 8 h at room temperature. The product was filtered, washed with de-ionized water and dried. For the PANI/ /Ag–Pd nanocomposite, 1 mL of 0.02 M $AgNO_3$ was mixed with 2 mL of 0.062 M hydrazine and stirred at 60 °C for 5 min. Then, 50 mL of 0.035 M $PdCl_2$ was added and stirred for 45 min. Finally, 10 mL of the Ag–Pd solution was mixed with 0.05 g PANI and 10 mL APS, followed by filtration, washing with de-ionized water and vacuum drying at 60 °C for 12 h.

EY dye degradation

The degradation of EY dye was evaluated by monitoring the decrease in its characteristic absorbance peak using a UV–Vis spectrophotometer (Jasco V-530 UV–Vis spectrophotometer) in the range of 350–800 nm. Pure dimethylformamide (DMF) was used as the blank solvent to eliminate background interference. Absorbance was converted into concentration using a calibration curve as suggested in a previous study.[31] Degradation efficiency was calculated from the relative decrease in absorbance with time according to Eq. (1). It was assessed under varying experimental conditions, including pH 1–11, nanocomposite dose, 0.5–1.5 mg/L, initial EY dye concentration, 3–12 mg/L, and reaction time, 5–15 s. The selected pH range is closely reported in previously published data, to study its significance:[32,33]

$$\text{EY dye degradation} = 100\frac{c_0 - c_e}{c_e} \tag{1}$$

where c_0 and c_e are initial and equilibrium EY dye concentrations (mg/L).

Characterization

The FTIR analysis of the PANI/Ag–Pd nanocomposite, mixed with KBr and pressed into pellets, was carried out using a Shimadzu 8400S (Japan) spectrometer. The measurements were taken within the wavenumber range from 4000 to 400 cm^{-1}, with a resolution of 4 cm^{-1}, to identify the functional groups present in the nanocomposite. Additionally, the surface morphology, particle size and elemental composition of the synthesized PANI/Ag–Pd nanocomposite were analyzed using a scanning electron microscope (SEM) equipped with an energy dispersive X-ray (EDX) system.

Experiments design

RSM was employed to assess the individual and interactive effects of four variables, *A* (pH), *B* (composite dose), *C* (EY concentration) and *D* (reaction time) on degradation efficiency using a bimetallic polyaniline/Ag–Pd nanocomposite. A central composite design (CCD) was applied to construct a three-level matrix with factors coded as –1 (low) and +1 (high). Variable levels are detailed in Table I.

TABLE I. Level of parameters for central composite design (CCD)

Variable	Symbol	Level	
		Low (–1)	High (1)
Dose of composite, mg/L	*A*	0.5	1.5
Dose of dye, mg/L	*B*	3	12
pH	*C*	1	11
Time, s	*D*	5	15

The response analysis was performed using Design Expert 13 through a regression-based approach. The main influences of the input variables are denoted as *A*, *B*, *C* and *D*, while their combined or interaction effects are represented by terms such as *AB*, *AC*, *AD*, *BC*, *BD* and *CD*, along with the quadratic components A^2 and B^2. The relationship between the variables and the response was modeled using a second-order polynomial equation:

$$Y = a_0 + \sum_{i=1}^{n} a_i X_i + \sum_{i=1}^{n} a_{ii} X_i^2 + \sum_{j=i+1}^{n} a_{ij} X_i X_j \quad (2)$$

Where Y is predicted response, X_i are independent variables, a_0 is constant (intercept), a_i are linear coefficients, a_{ii} are quadratic coefficients (squared terms) and a_{ij} are interaction coefficients (cross-product terms).

After each run, final concentration of EY dye was determined in order to find out the degradation in %.

RESULTS AND DISCUSSION

UV–Vis spectral analysis

The UV–Vis spectra (Fig. 1) reveal key optical features of pure PANI and the PANI/Ag–Pd nanocomposite. Pure PANI shows peaks at 283 and 342 nm, indicating its doped state. In the composite, the π–π* peak shifts to 293 nm and a new band at ~425 nm appears, attributed to Ag/Pd surface plasmon resonance. These changes confirm nanoparticle incorporation and improved optical properties, supporting its photocatalytic potential.

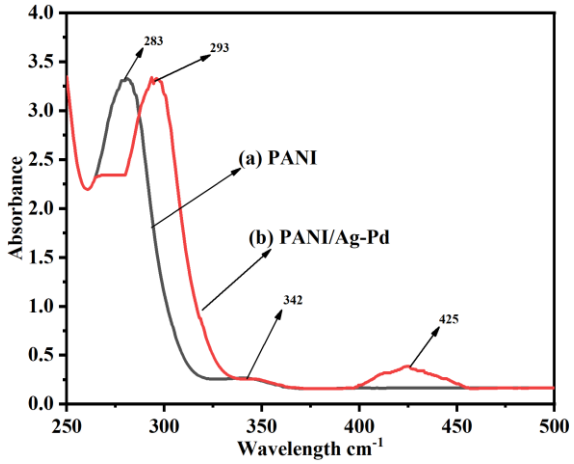

Fig. 1. UV–Vis analysis of: a) PANI and b) PANI/Ag–Pd.

FTIR analysis

The FTIR spectrum illustrates the structural differences between pure polyaniline (PANI) and the PANI/Ag–Pd nanocomposite, as shown in Fig. 2. The "a" spectrum corresponds to PANI, exhibiting characteristic peaks associated with its chemical structure. Notably, peaks in the ranges 1560–1580 and 1480–1500 cm^{-1}

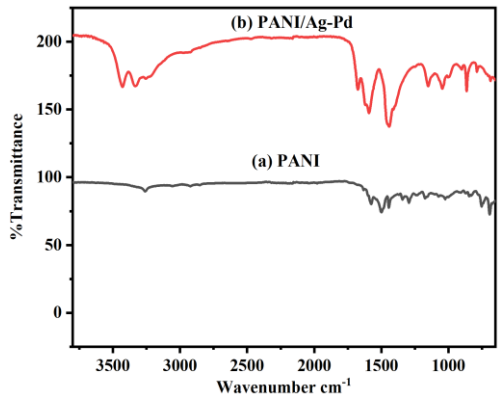

Fig. 2. FTIR analysis of: a) PANI/Ag–Pd and b) PANI.

are associated with the C=C stretching vibrations of the quinoid and benzenoid structures in the polymer chain. The absorption band close to 1300 cm^{-1} is attributed to C–N stretching, while the signal near 1140 cm^{-1} corresponds to the in-plane bending of aromatic C–H bonds, which is commonly connected to the electrical conductivity characteristics of PANI. In contrast, the "b" spectrum represents the PANI/Ag–Pd nanocomposite, which shows noticeable shifts in peak positions and variations in intensity, particularly in the 1500–1000 cm^{-1} region. These changes suggest strong interactions between the polyaniline matrix and the incorporated silver–palladium nanoparticles, likely through coordination with nitrogen atoms in the PANI backbone. The appearance of a broader peak near 3400 cm^{-1} may be attributed to N–H stretching or adsorbed water molecules. Overall, the spectral modifications confirm the successful incorporation of Ag–Pd nanoparticles into the PANI structure, potentially enhancing the composite's physicochemical properties for applications such as dye removal or catalytic activity.

Surface morphology characterization

SEM was employed for the measurement of surface morphology of PANI/Ag–Pd nanocomposite. The SEM images were taken at low and high resolution. These SEM images are shown in Fig. 3a and b at low and high resolutions. The

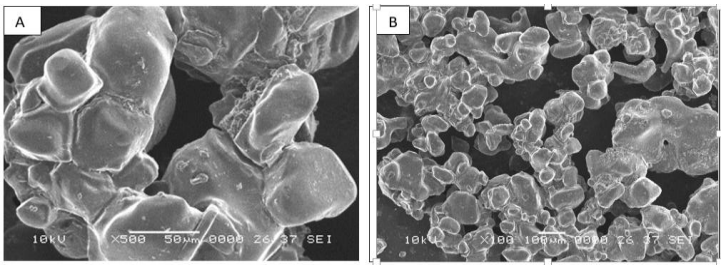

Fig. 3. The SEM images of: a) PANI and b) PANI/Ag–Pd.

SEM shows that structure of PANI/Ag–Pd nanocomposite is semi-cubical and white dots are present due to the presence of PANI/Ag–Pd nanocomposite. According to image, the silver and palladium particle were finely distributed within the PANI matrix, although some accumulation and agglomeration were observed in certain area.

EDX analysis

EDX analysis (Fig. 4) was employed to verify the elemental composition of the PANI/Ag–Pd nanocomposite. The spectrum displays distinct peaks corresponding to carbon, nitrogen and oxygen elements associated with the PANI matrix. Additionally, the presence of characteristic peaks for silver and palladium confirms the successful incorporation of metal nanoparticles into the composite structure in K-shell with 1.99, 1.86 and 33.97 %, respectively. Silver and palladium were found in L-shell with 49.93 and 12.23 %.

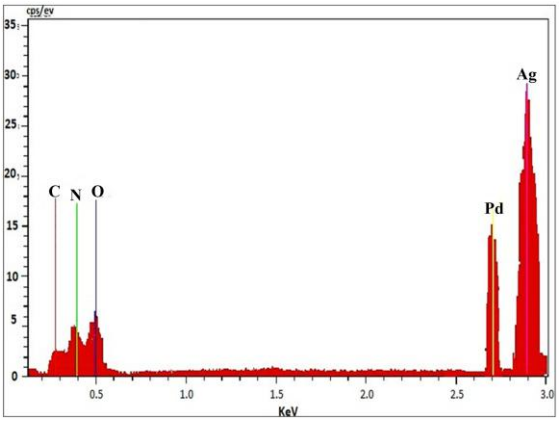

Fig. 4. EDX analysis of PANI/Ag–Pd nanocomposite.

EY dye degradation

A comparative parametric analysis was conducted to evaluate the effectiveness of various factors (pH, nanocomposite dose, initial dye concentration and reaction time) influencing the degradation of the EY dye using a PANI/Ag–Pd. The progressive degradation of the dye in the presence of PANI/Ag–Pd and $NaBH_4$ was monitored *via* UV–Vis spectroscopy, as illustrated in Fig. 5. The characteristic absorbance peak at approximately 336 nm exhibited a sharp decline with increasing reaction time, indicating a rapid reduction in dye concentration. At 5 s, the spectrum displayed the highest absorbance, corresponding to the initial dye concentration. Subsequent measurements at 10 s, showed a significant decrease in peak intensity, while the peak was almost diminished at 15 s, indicating almost total degradation. This continuous absorbance reduction witnesses

that UV–Vis spectroscopy effectively captured the real-time degradation behavior and highlights the efficiency of the PANI/Ag–Pd–$NaBH_4$ system, achieving most of dye removal within 15 s.

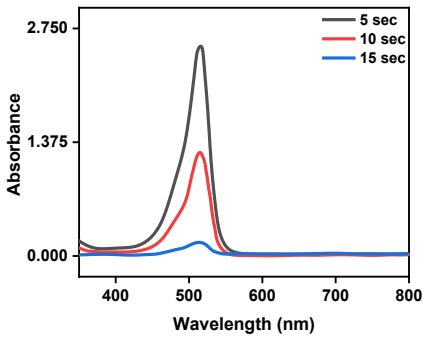

Fig. 5. UV–Vis spectra of dye degradation.

Experimental results revealed that a maximum degradation efficiency of 96.63 % was achieved under optimal conditions: pH 5.8, nanocomposite dose, 500 µg/L, initial EY dye concentration, 900 µg/L, and reaction time, 15 s; this was expected, as the integration of Ag–Pd enhances the availability of active binding sites, thereby improving the degradation efficiency.

Response surface model results

ANOVA and regression model results regression analysis was performed to predict EY dye degradation, considering factors *A*, *B*, *C* and *D*, along with their interactions (*AB*, *AC*, *AD*, *BC*, *BD*, *CD*), as summarized in Table II. The resulting equations show that positive coefficients indicate synergistic effects, while neg-

TABLE II. ANOVA for cubic model (response: EY dye degradation, %)

Source	Sum of squares	*Df*	Mean square	*F*-value	*p*-value	Significance
Model	16337.89	14	1166.99	102.39	< 0.0001	Significant
A-Dose of composite	85.97	1	85.97	7.54	0.0177	
B-Dose of EY	68.31	1	68.31	5.99	0.0307	
C-pH	2917.47	1	2917.47	255.96	< 0.0001	
D-Time	368.81	1	368.81	32.36	0.0001	
AB	0.0000	1	0.0000	0.0000	1.0000	
AC	123.19	1	123.19	10.81	0.0065	
AD	2.00	1	2.00	0.1756	0.6826	
BC	16.70	1	16.70	1.47	0.2494	
BD	7.428E-06	1	7.428E-06	6.517E-07	0.9994	
CD	361.48	1	361.48	31.71	0.0001	
A^2	127.14	1	127.14	11.15	0.0059	
B^2	13.58	1	13.58	1.19	0.2964	
C^2	10061.46	1	10061.46	882.74	< 0.0001	
D^2	204.33	1	204.33	17.93	0.0012	

ative ones suggest antagonistic impacts. These effects were analyzed to evaluate their influence on the model.

ANOVA for cubic model

The model demonstrates strong statistical significance, as indicated by a high *F*-value of 102.39 and a minimal probability (0.01 %), that this outcome is due to random variation. Variables *A*, *B*, *C* and *D*, as well as the interactions *AC*, *CD*, and the quadratic terms A^2, C^2 and D^2, significantly affect the response ($p < 0.0500$). In contrast, terms with *p*-values above 0.1000 are considered statistically insignificant. Removing these non-significant terms while maintaining model hierarchy can improve model performance. Additionally, the lack of fit test produced an *F*-value of 1.15 with a 41.59 % probability, suggesting it is not statistically significant relative to pure error.

In the Table III the predicted R^2 of 0.9482 is in reasonable agreement with the adjusted R^2 of 0.9920; *i.e.*, the difference is less than 0.2. This demonstrates a reasonable correlation between experimental and predicted results of EY dye degradation.

TABLE III. Regression model equation for response against factors and their interaction

Regression model equation	R^2	Adjusted R^2
EY dye degradation (%) = $98.90 - 2.61A - 2.50B + 26.74C - 11.10D + 0.0000AB + 3.37AC - 0.4868AD + 1.25BC + 0.0010BD + 11.13CD - 7.16A^2 + 1.09B^2 - 29.33C^2 - 11.52D^2$	0.9917	0.9820

Response contour plots

Fig. 6 presents contour plots from RSM analysis, showing the interaction effects of key variables on EY dye degradation (%). Each plot illustrates the combined impact of two factors while keeping others constant. A color gradient from blue to red indicates increasing degradation efficiency. Results show that higher composite doses and lower pH levels significantly enhance degradation due to more active sites and increased $^{\bullet}OH$ generation. In contrast, higher dye concentrations reduce efficiency.

Performance evaluation of model

Performance of model was evaluated by predicted vs. actual plot which visual representation of a model's accuracy, commonly used in regression analysis and machine learning to assess predictive performance.

In Fig. 7 the data points in this plot closely align with the diagonal line, indicating that the model has high accuracy and reliability in predicting EY dye degradation. The smooth color gradient suggests a well-fitted model without significant fluctuations and provides strong predictive performance for EY dye degradation.

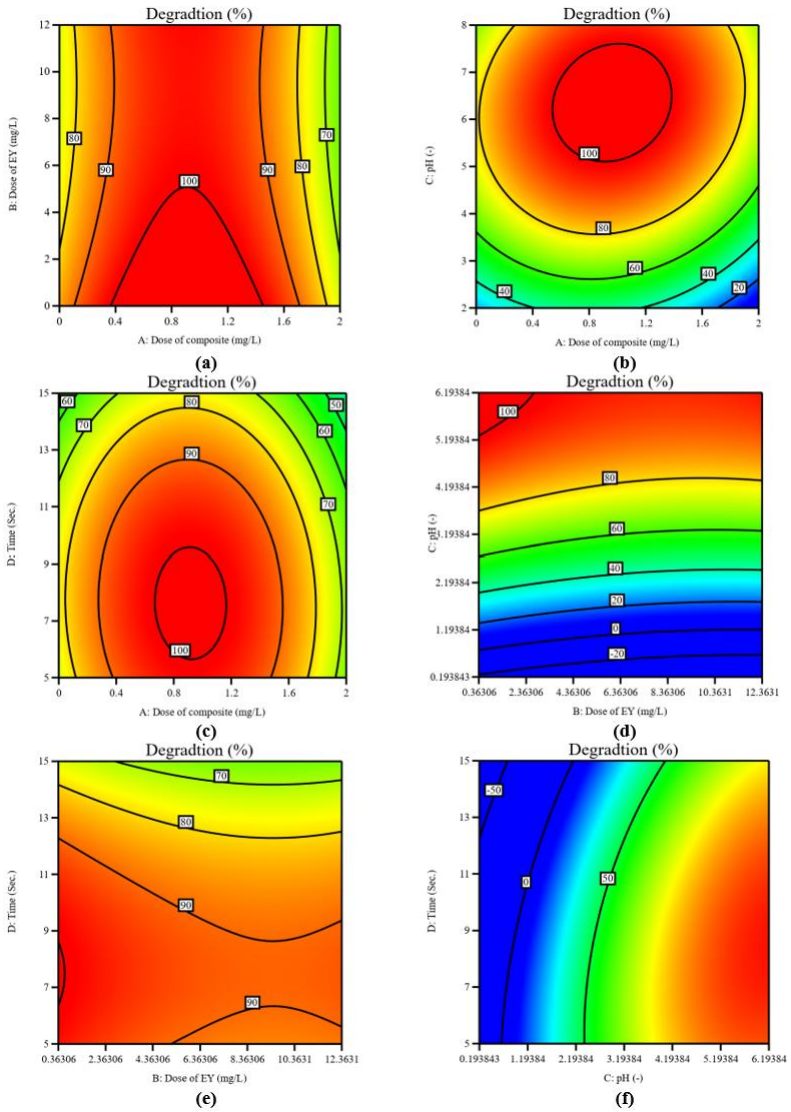

Fig. 6. Contour plots of performance evaluation: a) dose of composite and dose of EY, b) dose of composite and pH, c) dose of composite and time, d) dose of EYand time, e) Dose of EY and time and f) pH and time.

Optimization of exponential parameters

Fig. 8 presents the optimized conditions for maximizing EY dye degradation using a composite, based on desirability function analysis from an RSM model. In solution 34 (out of 100), the optimal composite dose is 1.42706 mg/L and the EY concentration is 3.22423 mg/L, indicating that higher composite loading and

lower dye concentration enhance degradation. The optimal pH is 5.80, favoring dye–composite interaction, and the reaction time is short (6.01 min), showing rapid degradation. This setup achieves 99.69 % efficiency with a desirability value of 1.000, making it highly effective for wastewater treatment.

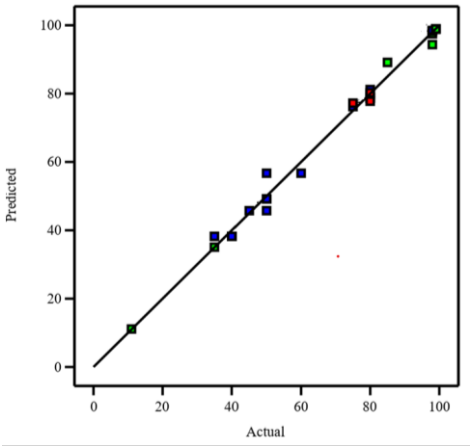

Fig. 7. Actual and predicted performance of model for EY dye degradation.

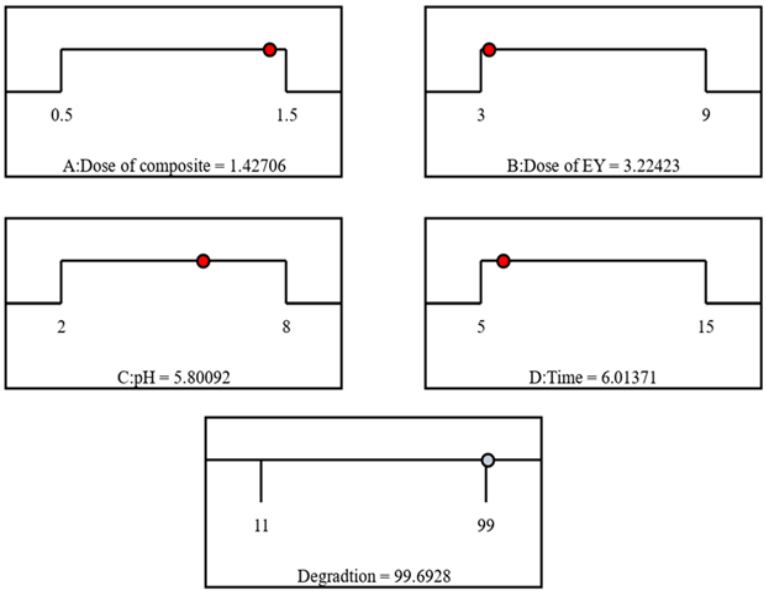

Fig. 8. Optimization of experimental parameter using PANI/Ag–Pd.

Comparison of EY dye degradation

The results of dye degradation obtained in this study are benchmarked with those reported in previous literature. This comparative analysis (summarized in

Table IV) highlights the potential of presently used PANI/Ag–Pd nanocomposite towards achieving the remarkable dye removal (96.63 %) which can be attributed to the synergistic interaction between polyaniline and bimetallic Ag–Pd nanoparticles. While previous studies demonstrated the lower degradation efficiencies ranging from 92.30 to 99 %. However, these traditional composites require high material consumption and extended processing times. In contrast, the PANI/Ag––Pd system offers a rapid, energy-efficient and environmentally sustainable solution. Its low catalyst loading and ultrafast activity highlight its potential scalability for practical wastewater treatment. Future research should examine the stability and recyclability of this nanocomposite in real effluent conditions to confirm its applicability at industrial scale.

TABLE IV. Comparison of degradation of EY dye with earlier work reported

Composite	Dose of composite, mg/L	Time s	Dye dose mg/L	Degradation %	Ref.
Poly(pyrrole-co-aniline)-coated TiO_2/nanocellulose composite (P(Py-co-An)–TiO_2/NCC)	3500	5400	23.45	92.30	[34]
New gold Salen complex doped carbon nanocomposite (Au–Salen/CC)	5000	3000	0.27	98.68	[35]
TiO_2/tetra phenyl-porphyrin sulfonic acid nanocomposite (TiO_2/TPPS)	1100	3000	10.0	99.00	[36]
PANI/Ag–Pd nanocomposite	1.42	360.6	3.0	96.63	This study

CONCLUSION

The study showed that PANI/Ag–Pd nanoparticles significantly enhance the degradation of eosin yellow (EY) dye. Characterization *via* UV–Vis, FTIR, SEM and EDX confirmed successful synthesis of the nanocomposite. Using central composite design with response surface methodology (RSM), optimal conditions 1.42706 mg/L composite dose, EY dose, 3.22423 mg/L, pH 5.80 and 6.01 min yielded 96.6 % degradation. These results highlight the nanocomposite's high catalytic efficiency and the effectiveness of RSM for process optimization in wastewater treatment. This work highlights the practical and environmental relevance of the PANI/Ag–Pd nanocomposite as a rapid, energy-efficient and sustainable material for wastewater remediation, offering a green alternative for treating dye-contaminated effluents. The ability to achieve such high degradation within seconds under mild conditions demonstrates its potential scalability for industrial applications. Future research should focus on long-term stability, recyclability, performance in real industrial wastewater and the extension of this approach to other toxic pollutants, thereby advancing the practical implement-

ation of nanocomposite-based catalytic systems in sustainable wastewater management.

И З В О Д

БИМЕТАЛНИ ПОЛИАНИЛИН/СРЕБРО–ПАЛАДИЈУМ НАНОКОМПОЗИТ ЗА БРЗУ И ОДРЖИВУ ДЕГРАДАЦИЈУ ЕОЗИН ЖУТЕ БОЈЕ ИЗ ОТПАДНИХ ВОДА

NOOR ZAMAN[1], FARAH NAZ TALPUR[1], ABDUL QADEER LAGHARI[2], JAMEEL BAIG[1], ARSHAD IQBAL[3], SHOUKAT ALI NOONARI[4], ZULFIQAR ALI BHATTI[2], AMANA BALOCH[1], IMRAN HASSAN AFARIDI[1] и MASROOR ABRO[2]

[1]National center of Excellence in Analytical chemistry, University of Sindh, Jamshoro, Sindh, Pakistan, [2]Process Simulation and Modeling Research Group, Chemical Engineering Department, Mehran University of Engineering and Technology Jamshoro, Sindh, Pakistan, [3]Chemical Engineering Department, Dawood University of Engineering and Technology, Karachi, Pakistan и [4]Department of Mechanical Engineering, Isra University, Hyderabad, Sindh, Pakistan

Еозин жута (EY) синтетичка ксантонска боја је високо токсична, што представља озбиљну претњу људском здрављу и воденим срединама. Хронично излагање EY може довести до иритације коже, респираторних поремећаја и потенцијалног дугорочног оштећења органа због његове упорне и биоакумулативне природе. У овој студији, нанокомпозит сребра и паладијума на бази полианилина (PANI/Ag–Pd) синтетизован је методом ко-таложења и коришћен као ефикасан нанокатализатор за разградњу EY боје. Структурне, морфолошке и елементалне особине синтетизованог нанокомпозита су окарактерисане коришћењем UV–Vis спектроскопије, Фуријe-трансформисане инфрацрвене спектроскопије (FTIR), скенирајуће електронске микроскопије (SEM) и енергетски дисперзивне спектроскопије X-зрака (EDX). UV–Vis и FTIR анализе су потврдиле формирање PANI/Ag–Pd нанокомпозита са значајним црвеним помаком, што указује на електронску интеракцију између састојака. SEM слике су показале успешну уградњу Ag и Pd наночестица у PANI матрицу, док је EDX потврдио је елементални састав. Нанокомпозит је показао изванредне фотокаталитичке перформансе под микроталасним зрачењем, постижући до 96,63 % деградације боје EY. Ова студија наглашава потенцијал PANI/Ag–Pd нанокомпозита као обећавајућих нанокатализатора за пречишћавање воде. Ови налази доприносе развоју наноматеријала стабилизованих полимером као ефикасних кандидата за санацију отпадних вода контаминираних бојом.

(Примљено 2. јула, ревидирано 14. августа, прихваћено 1. октобра 2025)

REFERENCES

1. M. M. Shameem, S. Sasikanth, R. Annamalai,R. G. Raman, *Mater. Today: Proc.* **45** (2021) 2536 (https://doi.org/10.1016/j.matpr.2020.11.254)
2. N. F. Alheety, A. H. Majeed,M. A. Alheety. *J. Phys.: Conf. Ser.* **1294** (2019) 052026 (https://doi.org/10.1088/1742-6596/1294/5/052026)
3. A. Kamal, M. Ashmawy, S. S, A. M. Algazzar, A. H. Elsheikh, *Proc. Inst. Mech. Eng., C* **236** (2022) 4843 (https://doi.org/10.1177/09544062211055662)
4. L. A. Adnan, N. F. Alheety, A. H. Majeed, M. A. Alheety, H. Akbaş, *Mater. Today: Proc.* **42** (2021) 2700 (https://doi.org/10.1016/j.matpr.2020.12.707)
5. S. El Harfi, A. El Harfi, *Appl. J. Environ. Eng. Sci*. **3** (2017) 311 (https://doi.org/10.48422/IMIST.PRSM/ajees-v3i3.9681)
6. P. Zarrintaj, M. K. Yazdi, H. Vahabi, P. N. Moghadam, M. R. Saeb, *Prog. Org. Coat.* **130** (2019) 144 (https://doi.org/10.1016/j.porgcoat.2019.01.053)

7. M. Berradi, R. Hsissou, M. Khudhair, M. Assouag, O. Cherkaoui, A. El Bachiri, A. El Harfi, *Heliyon* **5** (2019) e02711 (https://doi.org/10.1016/j.heliyon.2019.e02711)
8. A. Kausar, M. Iqbal, A. Javed, K. Aftab, Z.-i.-H. Nazli, H. N. Bhatti, S. Nouren, *J. Mol. Liq.* **256** (2018) 395 (https://doi.org/10.1016/j.molliq.2018.02.034)
9. E. Forgacs, T. Cserháti, G. Oros, *Environ. Int.* **30** (2004) 953 (https://doi.org/10.1016/j.envint.2004.02.001)
10. I. Ullah, A. Haider, N. Khalid, S. Ali, S. Ahmed, Y. Khan, N. Ahmed, M. Zubair, *Spectrochim. Acta, A* **204** (2018) 150 (https://doi.org/10.1016/j.saa.2018.06.046)
11. X. Muñoz, D. Clofent, M. J. Cruz, *Curr. Opin. Allergy Clin. Immunol.* **23** (2023) 70 (https://doi.org/10.1097/aci.0000000000000885)
12. S. Shahabuddin, R. Khanam, M. Khalid, N. M. Sarih, J. J. Ching, S. Mohamad, R. Saidur, *Arabian J. Chem.* **11** (2018) 1000 (https://doi.org/10.1016/j.arabjc.2018.05.004)
13. S. Rafaqat, N. Ali, C. Torres, B. Rittmann, *RSC Adv.* **12** (2022) 17104 (https://doi.org/10.1039/D2RA01831D)
14. S. Khan, T. Noor, N. Iqbal, L. Yaqoob, *ACS Omega* **9** (2024) 21751 (https://doi.org/10.1021/acsomega.4c00887)
15. S. Dutta, B. Gupta, S. K. Srivastava, A. K. Gupta, *Mater. Adv.* **2** (2021) 4497 (https://doi.org/10.1039/D1MA00354B)
16. S. Goudjil, S. Guergazi, T. Masmoudi, S. Achour, *Desalin. Water Treat.* **209** (2021) 429 (https://doi.org/10.5004/dwt.2021.26474)
17. R. Zhao, S. Zong, Q. Ma, Z. Xu, J. Yuan, *Sci. Rep.* **15** (2025) 6306 (https://doi.org/10.1038/s41598-024-75153-2)
18. T. Cui, X. Wang, Y. Chen, Y. Chen, B. Fu, Y. Tu, *Water Resour. Ind.* **30** (2023) 100217 (https://doi.org/10.1016/j.wri.2023.100217)
19. G. Zeng, X. Liu, L. Wu, Z. Meng, D. Zeng, C. Yu, *Chin. J. Struct. Chem.* **43** (2024) 100462 (https://doi.org/10.1016/j.cjsc.2024.100462)
20. F. J. Benitez, J. L. Acero, F. J. Real, *J. Hazard. Mater.* **89** (2002) 51 (https://doi.org/10.1016/S0304-3894(01)00300-4)
21. K. Rajeshwar, M. Osugi, W. Chanmanee, C. Chenthamarakshan, M. V. B. Zanoni, P. Kajitvichyanukul,R. Krishnan-Ayer, *J. Photochem. Photobiol., C* **9** (2008) 171 (https://doi.org/10.1016/j.jphotochemrev.2008.09.001)
22. V. K. Gupta, R. Saravanan, S. Agarwal, F. Gracia, M. M. Khan, J. Qin, R. V. Mangalaraja, *J. Mol. Liq.* **232** (2017) 423 (https://doi.org/10.1016/j.molliq.2017.02.095)
23. A. H. Majeed, L. A. Mohammed, O. G. Hammoodi, S. Sehgal, M. A. Alheety, K. K. Saxena, S. A. Dadoosh, I. K. Mohammed, M. M. Jasim, N. U. Salmaan, *Int. J. Polym. Sci.* **2022** (2022) 9047554 (https://doi.org/10.1155/2022/9047554)
24. J. Luo, S. Jiang, R. Liu, Y. Zhang, X. Liu, *Electrochim. Acta* **96** (2013) 103 (https://doi.org/10.1016/j.electacta.2013.02.072)
25. M. Deyab, G. Mele, E. Bloise, Q. Mohsen, *Sci. Rep.* **11** (2021) 12371 (https://doi.org/10.1038/s41598-021-91688-0)
26. J. Upadhyay, T. M. Das, R. Borah, *Int. J. Polym. Anal. Charact.* **26** (2021) 354 (https://doi.org/10.1080/1023666X.2021.1891799)
27. C. Abdul Kadar, M. Faisal, N. Maruthi, N. Raghavendra, B. Prasanna, S. Manohara, *Macromol. Res.* **30** (2022) 638 (https://doi.org/10.1007/s13233-022-0067-z)
28. A. Samadi, M. Xie, J. Li, H. Shon, C. Zheng, S. Zhao, *Chem. Eng. J.* **418** (2021) 129425 (https://doi.org/10.1016/j.cej.2021.129425)

29. R. Jamal, L. Zhang, M. Wang, Q. Zhao, T. Abdiryim, *Prog. Nat. Sci.: Mater. Int.* **26** (2016) 32 (https://doi.org/10.1016/j.pnsc.2016.01.001)
30. G. Gustafsson, Y. Cao, G. M. Treacy, F. Klavetter, N. Colaneri, A. J. Heeger, *Nature* **357** (1992) 477 (https://doi.org/10.1038/357477a0)
31. T. Anirudhan, S. Rejeena, *J. Mater.* **2015** (2015) 636409 (https://doi.org/10.1155/2015/636409)
32. V. J. Mayani, S. V. Mayani, S. W. Kim, *Sci. Rep.* **7** (2017) 7239 (https://doi.org/10.1038/s41598-017-07707-6)
33. R. Manivannan, J. Ryu, Y.-A. Son, *Colloids Surfaces, A* **608** (2021) 125601 (https://doi.org/10.1016/j.colsurfa.2020.125601).